A hybrid XFEM - Phase Field (*Xfield*) method for crack propagation in brittle materials

BIANCA GIOVANARDI[♯], ANNA SCOTTI[♯], and LUCA FORMAGGIA[♯]

October 18, 2016

[♯] MOX– Modellistica e Calcolo Scientifico
Dipartimento di Matematica
Politecnico di Milano
via Bonardi 9, 20133 Milano, Italy
bianca.giovanardi@polimi.it
anna.scotti@polimi.it
luca.formaggia@polimi.it

Keywords: Phase Field, XFEM, brittle fracture, crack propagation.

Abstract

The present work proposes a novel method for the simulation of crack propagation in brittle elastic materials that combines two of the most popular approaches in literature. A large scale displacement solution is obtained with the well known extended finite elements method (XFEM), while propagation is governed by the solution of a local phase field problem at the tip scale. The method, which we will refer to as *Xfield*, is here introduced and tested in 2D under mixed modes I and II loads. The main features and the capability of the Xfield to efficiently simulate crack propagation are shown in some numerical tests.

1 Introduction

Many methods are available to date to model and simulate propagation of fractures. Based on linear elastic fracture mechanics, the eXtended Finite Elements Method (XFEM) is currently one of the most popular methods to discretize the governing equations for the displacement evolution in brittle materials in the presence of one or more fractures. This method considers the fracture as a sharp one co-dimensional entity across which the displacement field is allowed to present a discontinuity, which should be accounted for in the numerical approximation of the momentum balance equation. The XFEM was first proposed by Belytschko and Black in [1], and later improved by Moes, Dolbow, and Belytschko in [2], to avoid the mesh refinement that is necessary to conform the geometry of the mesh to that of the crack faces and to properly describe the near tip displacement field. The main idea of the XFEM is to include in the approximation

the information obtained from the analytical linear elastic fracture mechanics near tip solution, by adding to the finite elements space some extra functions that mimic the analytical behavior of the solution of the problem. Though the XFEM was originally developed for applications concerning fractures, it has been later extended to several other applications, including, for example, two-phase flow [3] [4] and fluid structure interaction [5]. A classical approach to simulate the propagation of a fracture consists in a split strategy where displacement, strain and stress fields are first determined with the XFEM and then used for the evaluation of the stress intensity factors [22], the energy release rate [25], or the J-integral [27], depending on which criterion is chosen to determine the extent and direction of crack propagation. However, even if an XFEM discretization efficiently computes the displacement field in a material with a given fracture, a rigorous theory to predict whether a crack propagates or initiates, and the orientation of the new crack segments, is still missing. Moreover, it is still unclear how to determine the velocity of the propagation [6].

In a different manner, an energetic reformulation of the problem [7, 8] allows to derive an alternative model, which considers the crack as a smooth transition from the uncracked to the cracked states of the material, represented by the values of a phase field variable. The numerical approximation in this case is straightforward and does not require extra tools to handle the fracture [9, 10], which propagates along a path of least energy. The phase field model incorporates the fracture evolution in the equations, at the price of a high computational cost. Indeed, a characteristic length scale is introduced, which affects the choice of the mesh size. Moreover, the model consists of a system of nonlinearly coupled equations for two fields, namely the displacement and the phase field. Recent works aimed at making phase field simulations more affordable are in the direction of isotropic [32] and anisotropic [33] mesh adaptation and of massive parallelization [11]. In addition to the high computational cost, phase field models have another drawback. Indeed, we believe the enforced continuity of the displacement field in the presence of a crack is limiting in all those applications that require an explicit description of the crack opening, such as in the simulation of pressurized fractures, where the crack is the domain of a fluid flow and crack opening affects the permeability of the fracture. Hydraulic fracture is currently being studied both with phase field [12] and with XFEM [13] based approaches.

The aim of this work is to design a new method for the simulation of crack propagation in brittle elastic materials. The novel method that we propose here is intended to provide an explicit description of the crack opening, while using an energy based criterion for propagation. Moreover, the method is designed to be less computationally expensive than the phase field, by optimizing the the computational effort. Indeed, since the XFEM allows for the efficient computation of the displacement when the fracture geometry is given, and the variational approach is able to predict the crack path even in complex topologies, the strategy that we propose consists in limiting the use the phase field just to propagate the crack, and using the XFEM to compute the displacement field. As in [14], where a damage model is combined with the XFEM to support the prediction of crack path, in our implementation a sharp and a smeared description of the crack coexist. In particular, we propose a strategy in which the phase field solution

is used as a mathematically sound criterion for crack propagation.

The paper is structured as follows. In Section 2 the governing equations are stated, while in Section 3 the two approaches based on the XFEM and on the phase field are reviewed. Section 4 compares the solutions obtained with the XFEM and with a finite element discretization of the phase field model for a simple configuration of one crack under mode I load, highlighting the advantages and drawbacks of both strategies. In Section 5 we detail the implementation of the Xfield method, while the main features and the capability of the Xfield to efficiently simulate crack propagation are shown in a few numerical tests in Section 6. Conclusions are finally drawn in Section 7.

2 The governing equations

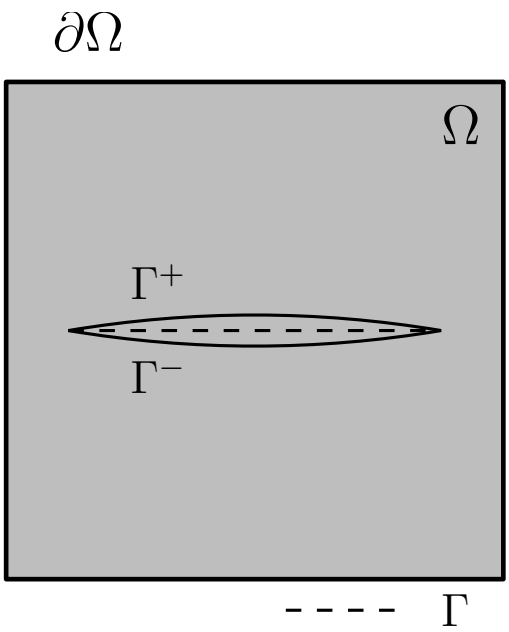

Figure 1: *The domain Ω and the initial crack. The two lips of the crack are referred to as Γ^+ and Γ^-, while the external boundary is $\partial\Omega$. Finally, Γ is the center line of the crack.*

Let Ω a two dimensional domain filled with a linear elastic material that presents a crack. Let Γ^+ and Γ^- the two lips of the crack, and Γ its center line. We want to predict the propagation of the crack, under given loading conditions. Being $\boldsymbol{u}$ the displacement field in the material and $\boldsymbol{\sigma}(\boldsymbol{u})$ the Cauchy stress tensor, the equations that describe the momentum balance are the following:

$$
\begin{cases}
\nabla \cdot \boldsymbol{\sigma}(\boldsymbol{u}) = \boldsymbol{f} & \text{in } \Omega, \\
\boldsymbol{\sigma}(\boldsymbol{u})\, \boldsymbol{n} = \boldsymbol{0} & \text{on } \Gamma^+ \cup \Gamma^-, \\
\boldsymbol{\sigma}(\boldsymbol{u})\, \boldsymbol{n} = \boldsymbol{t} & \text{on } \Gamma_t, \\
\boldsymbol{u} = \boldsymbol{g} & \text{on } \Gamma_u,
\end{cases}
\tag{1}
$$

where Γ_t and Γ_u are a partition of the external boundary $\partial\Omega$, $\boldsymbol{n}$ is the outwards normal vector, and $|\Gamma_u| > 0$. Here, $\boldsymbol{t}$ and $\boldsymbol{g}$ are the prescribed boundary conditions, in terms of traction and displacement, respectively. Notice that we are assuming the separation of the crack lips, and no cohesive behavior is considered in the present work.

From now on, we will assume the absence of body forces, that is $\boldsymbol{f} = \boldsymbol{0}$.

According to Hooke's Law, the stress tensor can be written as

$$\boldsymbol{\sigma}(\boldsymbol{u}) := \lambda\, tr\, \boldsymbol{\varepsilon}(\boldsymbol{u})\boldsymbol{I} + 2\mu\boldsymbol{\varepsilon}(\boldsymbol{u}),$$

where $\boldsymbol{\varepsilon}(\boldsymbol{u}) := \nabla_s \boldsymbol{u}$ is the strain, being $\nabla_s \boldsymbol{u}$ the symmetric part of $\nabla \boldsymbol{u}$, and λ and μ are the first and second Lamé parameters. The elastic energy density in Ω is, then,

$$\psi_e = \frac{1}{2}\boldsymbol{\sigma} : \boldsymbol{\varepsilon}.$$

The momentum balance equation in System (1), completed with the boundary conditions and with the constitutive relation of linear elasticity, allows to compute the displacement field. According to linear elastic fracture mechanics, the stress distribution corresponding to that displacement field determines whether the loading conditions allow for the growth of the crack or not.

3 Xfem and Phase Field: Two opposite approaches

In this section, we describe two possible strategies to simulate crack propagation, based on different representations of the crack (Figure 2). The first approach considers the fracture as a sharp entity on which the displacement field is allowed to be discontinuous. The numerical approximation of the equations (1) has to account for the discontinuity of the solution across the fracture, and a discretization method that is often used to this aim is the XFEM [1, 2]. The second approach consists in a reformulation of the problem in terms of energy minimization. The evolution of the system is driven by the minimization of the energy functional with respect to the admissible displacements and to the fracture itself. In this case, the fracture is represented by a variable called *phase field*, which varies smoothly between the unbroken and the broken states of the material. The crack is considered a smeared entity represented by some value of the phase field and its path is a natural outcome of the analysis.

3.1 XFEM

The main idea of the XFEM is to include in the discretization the information gained by an asymptotic study of the near-tip displacement solution and by the *a priori* observation of the displacement jump across the crack. In the XFEM some degrees of

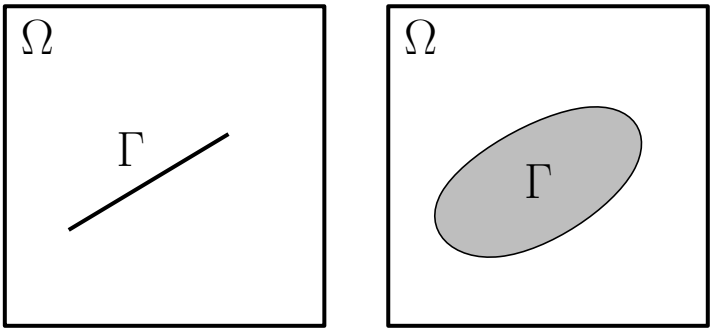

Figure 2: A sketch of a cracked domain Ω. On the left, the crack is represented as a lower dimensional entity, while, on the right, the crack is defined in a smeared sense.

freedom are added to enrich a standard finite elements space with discontinuous functions across the crack and with near-tip asymptotic functions. The main advantage of the XFEM with respect to the classical finite element method for the simulation of crack propagation is that the mesh does not need to match the geometry of the fracture and the problem of remeshing the domain as the crack grows is avoided. Indeed, the crack geometry is modeled independently of the underlying mesh, and a crack is simply grown by redefining the tip location and adding new crack segments.

The crack path may be represented explicitly with piece-wise straight crack segments, or with other techniques such as level sets. XFEM has been mainly applied to problems involving a few cracks, except for a few works, e.g. [15] [16]. Complex patterns, such as branching or intersection, have been considered in [17] and [18]. However in these cases, formulation and implementation become cumbersome, as well as in case of 3D geometries [19], [20].

The weak formulation of System (1) is described in [2] and here reported for the sake of completeness. The space of the admissible displacement fields is

$$\mathcal{U} := \{\boldsymbol{v} \in V : \boldsymbol{v} = \boldsymbol{g} \text{ on } \Gamma_u, \text{ and } \boldsymbol{v} \text{ is discontinuous on } \Gamma\},$$

and the space of the test functions is

$$\mathcal{U}_0 := \{\boldsymbol{v} \in V : \boldsymbol{v} = \boldsymbol{0} \text{ on } \Gamma_u, \text{ and } \boldsymbol{v} \text{ is discontinuous on } \Gamma\},$$

where $V = \boldsymbol{H}^1(\Omega)$. The weak formulation, which can be shown to be equivalent to the strong form (6), is then

$$\text{Find } \boldsymbol{u} \in \mathcal{U} \text{ such that } \int_\Omega \boldsymbol{\sigma}(\boldsymbol{u}) : \boldsymbol{\varepsilon}(\boldsymbol{v}) \, \mathrm{d}\Omega = \int_{\Gamma_t} \boldsymbol{t} \cdot \boldsymbol{v} \, \mathrm{d}\Gamma \qquad \forall \boldsymbol{v} \in \mathcal{U}_0.$$

When building an approximation space of $\mathcal{U}_0$, it is natural to include discontinuous functions in the basis of the finite elements space by means of the Heaviside function H that changes sign across the crack. Moreover, it was shown [21] that the use of a tip enrichment leads to increased accuracy. This consists in the further addition of a set of

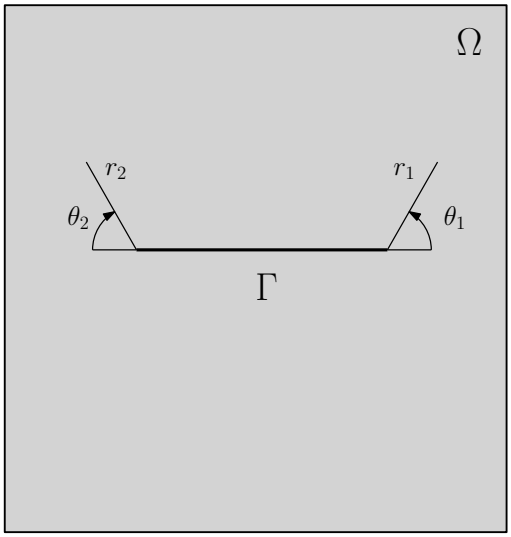

Figure 3: *The local polar coordinate systems at the tips.*

shape functions F_l^i, $i = 1, 2$, $l = 1, \ldots, 4$ that mimic the displacement $r^{1/2}$-behavior at the crack tip, which implies the $r^{-1/2}$-singularity of the stress.

The discretization of the displacement by means of the the XFEM then reads in 2D

$$\begin{aligned} \boldsymbol{u}_h(\boldsymbol{x}) = & \underbrace{\sum_{i \in I} u_i \boldsymbol{\phi}_i(\boldsymbol{x})}_{\text{Classical FE base}} + \underbrace{\sum_{j \in J} b_j H(\boldsymbol{x}) \boldsymbol{\phi}_j(\boldsymbol{x})}_{\text{Across crack enrichment}} \\ & \underbrace{+ \sum_{k \in K_1} \left(\sum_{l=1}^{4} c_k^{l,1} F_l^1(r_1, \theta_1) \right) \boldsymbol{\phi}_k(\boldsymbol{x}) + \sum_{k \in K_2} \left(\sum_{l=1}^{4} c_k^{l,2} F_l^2(r_2, \theta_2) \right) \boldsymbol{\phi}_k(\boldsymbol{x}),}_{\text{Near tip enrichment}} \end{aligned} \tag{2}$$

where the asymptotic crack tip functions F_l^i are

$$\left\{ \sqrt{r_i} \sin\left(\frac{\theta_i}{2}\right), \sqrt{r_i} \cos\left(\frac{\theta_i}{2}\right), \sqrt{r_i} \sin\left(\frac{\theta_i}{2}\right) \sin\theta_i, \sqrt{r_i} \cos\left(\frac{\theta_i}{2}\right) \cos\theta_i \right\},$$

and (r_i, θ_i) is the local polar coordinate system at the crack tip i, Figure 3.

The sets of nodes I, J, K_1, and K_2 in (2) contain, respectively: I, the classical mesh nodes, J, the nodes to be enriched with the discontinuous function, K_1 and K_2, the nodes to be enriched for the first and the second crack tip. See [2] for further details.

Once, the displacement field has been computed, one can check whether the stress field allows for crack propagation. Many empirical criteria are available based on the stress intensity factors, introduced by Irwin in [22] as a measure of the strength of the singularity of the stress at the crack tips. Indeed, they allow to determine whether the crack grows or does not, the growth direction θ_c, and the length increment l_c (or, equivalently, the crack tip velocity $\dot{l}$).

The most common criteria used in the case of mode I and mode II mixed loading are

(a) maximum circumferential tensile stress,

(b) minimum strain energy density,

(c) maximum energy release rate.

The *maximum circumferential tensile stress* [23] criterion states that the crack will propagate in the direction θ_c such that the circumferential stress at the tip is maximum, while the *minimum strain energy density* [24] is based on the idea that a crack propagates along the minimum resistance path. Finally, the *maximum energy release rate* criterion [25] allows the crack to propagate along the direction where the energetic dissipation is maximum. The three criteria state that the crack grows when the related quantity in the direction θ_c is higher than a threshold, which depends on the toughness G of the material.

Finally, it is necessary to define the extent of the crack growth. In many recent works, [1,2,6], the crack propagation velocity is considered as a user-defined parameter of the problem, possibly dependent on the stress intensity factors.

The application of these criteria requires the computation of the stress intensity factors $\mathcal{K}_I$ and $\mathcal{K}_{II}$. This can be done, for example, exploiting a trick proposed in [1,2] that consists in computing the J-integral in an auxiliary crack state. We recall that the J-integral, introduced by Rice in [27], was shown to represent the rate of decrease in potential energy for a virtual crack extension *dl* [26] and, for a general-mode in 2D, it is linked to the stress intensity factors through Rice's formula [27]

$$J = \frac{\mathcal{K}_I^2 + \mathcal{K}_{II}^2}{E'} + \frac{\mathcal{K}_{III}^2}{2\mu}, \tag{3}$$

where E' is the generalized Young modulus and it is equal to E in case of plane strain and to $\frac{E}{1-\nu^2}$ in case of plane stress.

3.2 Phase Field

Phase field models for the evolution of brittle fracture can be derived by energetic considerations. Given Γ as in the left hand side of Figure 2, the potential energy associated with System (1) can be written as

$$\mathcal{E}(\boldsymbol{u}) = \int_{\Omega\setminus\Gamma} \psi_e(\nabla \boldsymbol{u})\, d\Omega. \tag{4}$$

In [28], studying at an energetic level the criteria for crack growth, Griffith introduced in the energy balance a surface term U_Γ and defined as $\mathcal{G} := \frac{\partial U_\Gamma}{\partial l}$ the amount of energy dissipated in an increment *dl* of crack length. Griffith's criterion for crack growth stated that, to allow fracture growth, a critical value G of the dissipation should be reached. Furthermore, the cracked material could not dissipate more energy than this

critical value, and an irreversibility condition was stated. In [7], Francfort and Marigo reformulate Griffith's theory defining the surface energy as

$$U_\Gamma = \int_\Gamma G \, d\Gamma \tag{5}$$

and state that the system acts to minimize the following total energy functional

$$\mathcal{E}(\boldsymbol{u}, \Gamma) = \int_{\Omega \setminus \Gamma} \psi_e(\nabla \boldsymbol{u}) \, d\Omega + \int_\Gamma G \, d\Gamma, \tag{6}$$

with respect to both $\boldsymbol{u}$ and Γ under the irreversibility constraint that $\Gamma = \Gamma(t) \supset \bigcup_{s<t} \Gamma_s$.

Remark 1 *Since it can be shown that $\mathcal{G} = J$, the well known formula* (3) *represents an important link between the linear elastic fracture mechanics criteria for crack propagation mentioned in Section 3.1 and Griffith's criterion, which allows to perform a comparison of the two models.*

In [29], the existence of a continuous time evolution of this model in a time span $[0, T]$ is proved and in [9], by exploiting the well known theoretical result [30], a two-field energy functional is introduced, which Γ-converges in $L^2(\Omega)$ to (6).

More precisely, in [30] Ambrosio and Tortorelli propose an approximation $\mathcal{E}_\epsilon$ of the energy functional (6), which is more suitable for numerical computations. The Ambrosio-Tortorelli functional is given by

$$\mathcal{E}_\epsilon(\boldsymbol{u}, c) = \int_\Omega \left(\eta_\epsilon + c^2\right) \psi_e(\nabla \boldsymbol{u}) \, \mathrm{d}\Omega + \int_\Omega G \left(\frac{1}{2\epsilon}(1-c)^2 + \frac{\epsilon}{2}|\nabla c|^2 \right) \, \mathrm{d}\Omega, \tag{7}$$

where $(\boldsymbol{u}, c) \in \boldsymbol{H^1}(\Omega) \times H^1(\Omega)$, $0 \leq c \leq 1, 0 \leq \eta_\epsilon << \epsilon$.

The variable c plays the role of a control variable on the gradient of $\boldsymbol{u}$, and it represents Γ. The variable c is a phase-field that varies smoothly between the cracked state, where $c = 0$, and the uncracked one, where $c = 1$. The crack is then identified by a smooth field, instead of a sharp lower dimensional set. Note that the first integral of (7) can be interpreted as a regularization of the bulk elastic energy (4), and the second one can be interpreted as a regularization of the surface energy (5).

The parameter ϵ plays a key role in the definition of the energy and weights the contributions of the two terms

$$\int_\Omega |\nabla c|^2 \, d\boldsymbol{x} \quad \text{and} \quad \int_\Omega (1-c)^2 \, d\boldsymbol{x} \tag{8}$$

to the total energy $\mathcal{E}_\epsilon$. Indeed, the first integral in (8) is proportional to the area of the transition region, where the gradient of the phase field is high, while the second integral is proportional to the area of the region where the material is damaged, which is where $c << 1$. Figure 4 shows two different phase fields representing the same crack, obtained from the minimization of the energy $\mathcal{E}_\epsilon$ with two different values of ϵ.

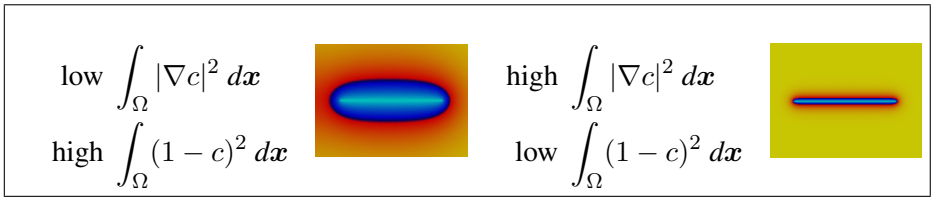

Figure 4: The phase field on the left is obtained with a larger ϵ than that on the right. A high ϵ makes it more favorable, in energetic terms, a configuration in which the crack is smeared over a bigger region, than a configuration in which the gradient of the phase field is higher.

The functional $\mathcal{E}(t)$ is proven to be approximated in the sense of Γ-convergence in $L^2(\Omega)$ by $\mathcal{E}_\epsilon$ as $\epsilon \to 0$ [30]. Moreover, it is shown in [31] that, as $\epsilon \to 0$, the quasi-static evolution $t \to (\boldsymbol{u}_\epsilon(t), c_\epsilon(t))$ of the functional $\mathcal{E}_\epsilon$ converges to the quasi-static evolution for brittle fracture detailed in [29], in the sense that there exists a sequence $\epsilon_n \to 0$ such that for all $t \in [0, T]$ one has

(a) $c_{\epsilon_n}(t)\nabla \boldsymbol{u}_{\epsilon_n}(t) \to \nabla \boldsymbol{u}(t)$ strongly in $L^2(\Omega)$,

(b) $\int_\Omega (\eta_{\epsilon_n} + c_{\epsilon_n}(t)^2)|\nabla \boldsymbol{u}_{\epsilon_n}(t)|^2 \, d\boldsymbol{x} \to \int_\Omega |\nabla \boldsymbol{u}(t)|^2 \, d\boldsymbol{x}$,

(c) $\int_\Omega G \left(\frac{\epsilon_n}{2}|\nabla c|^2 + \frac{1}{2\epsilon_n}(1-c)^2 \right) d\boldsymbol{x} \to \int_\Gamma G \, d\Gamma$.

Furthermore $\mathcal{E}_{\epsilon_n}(t) \to \mathcal{E}(t)$ for all $t \in [0, T]$.

By computing the first variation of the energy functional $\mathcal{E}_\epsilon$ with respect to $\boldsymbol{u}$ and c, we obtain the governing equations of the model. In particular,

$$\frac{\delta \mathcal{E}_\epsilon}{\delta \boldsymbol{u}} = \boldsymbol{0} \quad \Rightarrow \quad \nabla \cdot \tilde{\boldsymbol{\sigma}}(\boldsymbol{u}) = \boldsymbol{0} \quad \text{with} \quad \tilde{\boldsymbol{\sigma}}(\boldsymbol{u}) := c^2 \boldsymbol{\sigma}(\boldsymbol{u}), \tag{9}$$

$$\frac{\delta \mathcal{E}_\epsilon}{\delta c} = 0 \quad \Rightarrow \quad 2c\, \psi_e(\boldsymbol{u}) - G\epsilon\, \Delta c - \frac{G}{\epsilon}(1-c) = 0. \tag{10}$$

Equations (9) and (10) can be solved together as a system of nonlinearly coupled equations with standard finite elements, with particular care on the choice of the mesh size, which should be taken small enough so that the scale ϵ is properly resolved.

4 A motivation for Xfield

The XFEM approach described in Section 3.1 allows to efficiently and accurately compute the displacement field in a material with a given fracture but, to determining the propagation of the crack, it lacks a general and mathematically sound theory, as many different criteria are available to determine whether the crack grows and the growth direction, which may not give the same result in case of a realistic loading. Moreover, it is still unclear how to determine the propagation velocity [6].

On the other hand, the phase field approach of Section 3.2 has the advantage of incorporating the fracture evolution in the equations, but the computational cost of solving the two-field nonlinearly coupled system of equations (9) and (10) is high. Indeed, the characteristic length scale ϵ affects the choice of the mesh size, since a good numerical solution should be able to describe the gradient of the phase field, which is, close to the crack, of the order of $1/\epsilon$.

In particular, the computational mesh should be very fine in the region where we expect high gradients, that is along the crack and at the crack tip, as shown in Figure 5. Notice also, in Figure 5, that in most of the domain one has $\Delta c \approx 0$, implying that the solution of the phase field equation (10) reduces to the trivial equation

$$c = \frac{G}{G + 2\epsilon\psi_e}. \tag{11}$$

We point out that a discretization that does not involve a strong mesh refinement at the crack tip will fail in resolving crack propagation correctly, while a poor mesh resolution in the part of the crack far from the tip implies a poor representation of the gradient of c across the crack, leading to an unacceptable error in the numerical displacement field, as we will show in Section 4.1. A discretization strategy only based on mesh adaptation close to the crack would lead to an increase of the computational cost during the simulation, as the crack grows, while a method like the XFEM, which efficiently computes the displacement in the presence of a crack, allows to avoid a waste of resources on the portion of the crack that is far from the tip and to concentrate the numerical effort for the propagation just in the tip region.

In the present work we introduce the Xfield method as a valid alternative, in terms of computational effort, to mesh adaptation. The strategy that we are proposing is, indeed, to limit the use the phase field approach only to the purpose of propagating the crack, while computing the displacement field in the whole domain with the XFEM. In practice, the phase field solution is used as a mathematically sound criterion to propagate the crack, while the displacement field is efficiently computed on a reasonably coarse mesh with the XFEM. As a side effect, the Xfield bears the advantage of an explicit description of the displacement discontinuity, which can be useful when dealing with problems that explicitly need the crack opening, such as in the simulation of hydraulic fracturing.

4.1 A comparison of XFEM and Phase Field solutions on a test problem

We consider a square domain $\Omega = (0, b) \times (0, b)$ cut by a fracture $\Gamma = (0, b/2) \times b/2$, as shown in Figure 6. We compute the displacement field in the material when it is subject to a traction $\bar{\boldsymbol{\sigma}}$ at the top, and fixed at the bottom.

The problem is solved both with the XFEM, using linear finite elements for the displacement, and with the phase field, using linear finite elements for displacement and phase field. The mesh used in the XFEM solution is a uniform triangulation of elements of size $h = 30\ mm$, while the phase field is solved on two different meshes, both refined on an horizontal stripe that contains the fracture, whose element size near

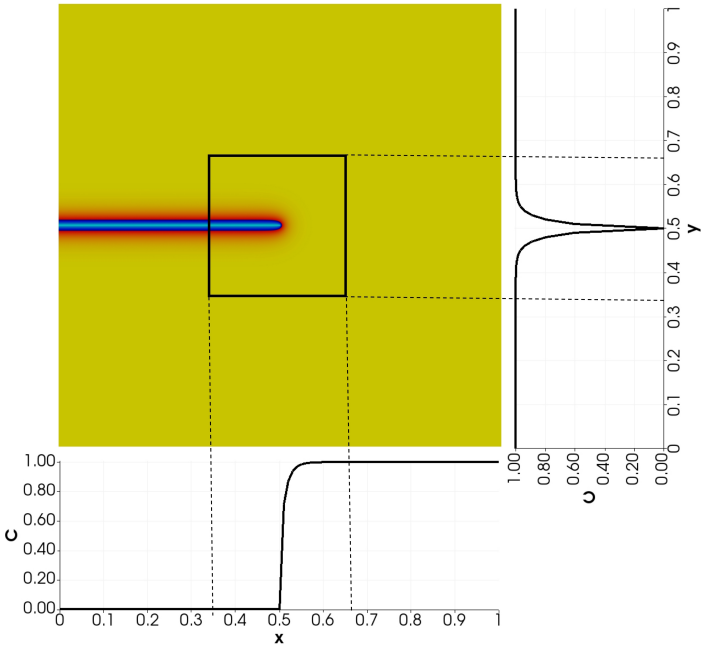

Figure 5: *The phase field representing a crack that cuts half of the domain. The phase field is projected along two lines (i.e. the horizontal center line at the bottom, and the vertical center line on the right) to show a typical profile of the phase field along and across the crack.*

the crack is $h = 3\ mm$ and $h = 0.5\ mm$ respectively. The results are shown in Figure 7.

It is clear from Figure 7 that the phase field method underestimates the displacement on the upper part of the domain, unless a very fine mesh is used. The reason for this behavior is that, unless enough elements are taken with respect to ϵ, the phase field model is unable to represent the failure of the material across the fracture, hence causing a spurious transmission of the stress across the fracture.

When studying the displacement field of a material with a given crack, the advantage, in terms of computational effort, of a sharp description of the crack with respect to the phase field is evident.

5 Implementation of the Xfield

The idea of the Xfield is to simulate crack propagation by approximating the displacement field on a reasonably coarse mesh with the XFEM and exploiting the solution of the nonlinear coupled problem of displacement and phase field locally at the crack tip as a propagation criterion. This allows us to focus the computational effort only at the tip, and, in particular, on a fine mesh that covers only a small part of the whole domain.

The implementation of this strategy requires special care in two main aspects.

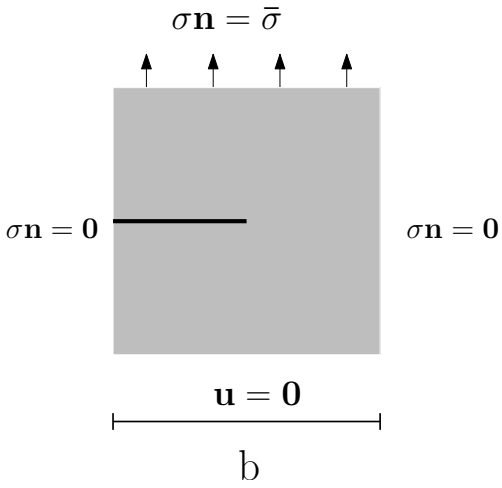

b	$1\,m$
λ	$120\,GPa$
μ	$80\,GPa$
G	$2700\,kN/m$
$\bar{\boldsymbol{\sigma}}$	$1\,MPa$
ϵ	$5\,10^{-2}\,m$

Figure 6: A sketch of the domain and boundary conditions. The parameters of the simulation are shown in the table.

- The displacement fields of equations (6) and (10), both indicated with $\boldsymbol{u}$ with a little abuse of notation, are different, as they are the solution of two different equations, and lead to two different elastic energies notably in the region where ∇c is high.
- The crack path should be tracked both by a level set function, which is used in the implementation of the XFEM, and with the phase field variable. Hence, a good strategy to update the level set, given the phase field, is needed.

For the sake of simplicity, we first give the implementation details in the easier case of propagation under mode I geometry and we extend later the method to mixed modes geometries.

5.1 The algorithm in the case of mode I propagation

We consider a crack under mode I loading, as shown in Figure 8. The domain Ω contains an initial crack and is subject to an increasing vertical displacement load. The bottom of the specimen is fixed.

In Figure 8, a small tip domain Ω_{tip}, whose boundary $\partial\Omega_{tip}$ is composed of the four edges γ_a, γ_b, γ_c, and γ_d, is centered at the crack tip and overlapped to Ω. Ω_{tip} is required to satisfy two assumptions.

1. Ω_{tip} is large enough that $\Delta c \approx 0$ on the edges of $\partial\Omega_{tip}$ that are not intersected by the crack (namely γ_b, γ_c, γ_d of Figure 5),
2. Ω_{tip} is large enough that, in one step of load increment, the crack propagates inside Ω_{tip}, so that the new tip of the crack is still inside Ω_{tip}.

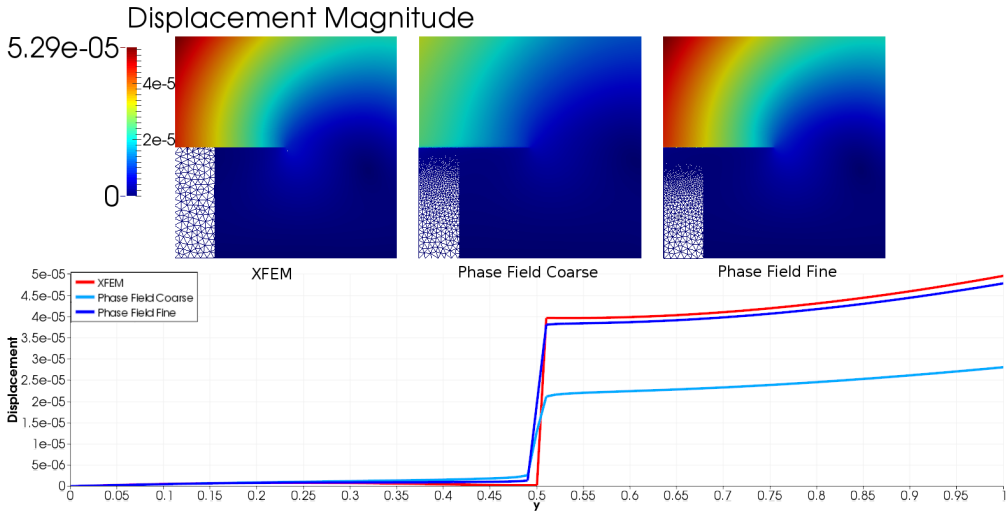

Figure 7: The displacement field obtained with the XFEM and with the phase field method on two different meshes. In the bottom left corners of the domains are shown the meshes employed in the simulations. Below, a plot of the diplacement field over a vertical line that intersects the fracture.

Under these assumptions, at a given load step, we obtain first the displacement with the XFEM on Ω. We then reconstruct this displacement on the boundary of Ω_{tip} and solve on Ω_{tip} the coupled problem of the displacement and phase field identified by equations (9) and (10), setting it as a boundary condition. This coupled problem on Ω_{tip} may be solved with a staggered scheme, as in [34], or with an alternate minimization algorithm, as in [9]. The extent of the tip domain Ω_{tip} is proportional to the length scale ϵ, so that a decrease of ϵ does not imply an increase of computational cost, but only a decrease of the tip domain extension, provided that Assumption 2. still holds.

Clearly, since a coupled problem of displacement and phase field will be solved near the tip, a proper set of boundary conditions should be specified on $\partial\Omega_{tip}$. As already mentioned, we require that the displacement on the boundary of the tip domain Ω_{tip} matches that obtained with the XFEM with continuity. We now address the conditions for the phase field. Due to the mode I geometry, it is reasonable to assume a homogeneous Neumann boundary condition on the edge γ_a that is crossed by the crack and on its opposite, that is γ_c. Furthermore, thanks to the first assumption on Ω_{tip}, we use (11) to set a Dirichlet boundary condition on the remaining part of the boundary, being ψ_e the elastic energy associated with the XFEM solution. Notice that, being the quantity $\epsilon\psi_e$ low away from the crack, the Dirichlet boundary condition set on the edges of $\partial\Omega_{tip}$ which are not intersected by the crack is close to 1.

In our implementation, the crack is represented as a set of segments and is updated by adding at each time iteration a new crack segment that links the previous crack with the current tip. To this purpose, it is necessary to localize the current crack tip $\boldsymbol{x}_{tip}^{n+1}$

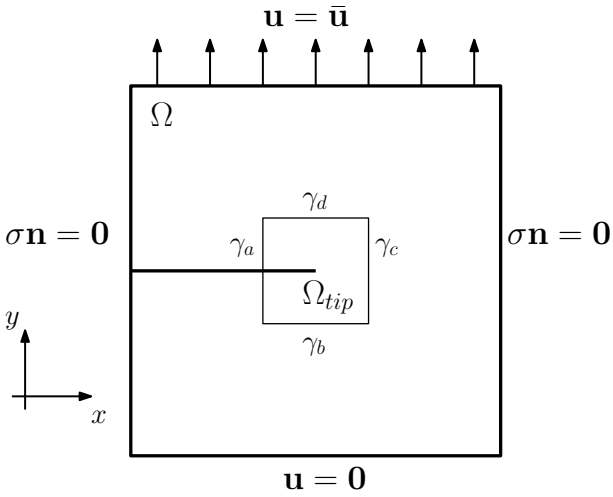

Figure 8: The domain Ω and a small region Ω_{tip} centered at the crack tip.

from the current phase field solution c. In the simple case of mode I propagation along the x direction, the localization of the new tip can be done by localizing the point where the gradient of c in the x direction is maximum, that is

$$\boldsymbol{x}_{tip}^{n+1} = \arg \max_{\boldsymbol{x} \in \Omega_{tip}} \nabla c(\boldsymbol{x}) \cdot \hat{\boldsymbol{x}}, \tag{12}$$

being $\hat{\boldsymbol{x}}$ the versor of direction x.

To sum up, the implementation of the Xfield with the staggered approach [34] is the following.

Being T the final time of the simulation, we use a constant time step $\Delta t = T/N$. At each time $t^n, \quad n = 0, \ldots, N-1$, given the current fracture Γ^n described by the phase field c^n, and the current tip domain Ω_{tip}^n, whose boundary $\partial\Omega^n$ is the union of γ_a^n, γ_b^n, γ_c^n, and γ_d^n, the following steps are performed:

(a) Compute $\boldsymbol{u}^{n+1}$ in Ω, by solving Problem (1) with the XFEM;

(b) Reconstruct $\boldsymbol{u}^{n+1}$ on $\partial\Omega_{tip}^n$ to get $\mathcal{I}_{\partial\Omega_{tip}^n}(\boldsymbol{u}^{n+1})$;

(c) Compute the displacement $\boldsymbol{u}_{tip}^{n+1}$ on Ω_{tip}^n, by solving the problem

$$\begin{cases} \nabla \cdot \left((c^n)^2 \boldsymbol{\sigma}(\boldsymbol{u}_{tip}^{n+1}) \right) = \mathbf{0} \text{ in } \Omega_{tip}^n \\ \boldsymbol{u}_{tip}^{n+1} = \mathcal{I}_{\partial\Omega_{tip}}(\boldsymbol{u}^{n+1}) \qquad \text{on } \partial\Omega_{tip}^n \end{cases}; \tag{13}$$

(d) Compute the phase field c^{n+1} in Ω^n_{tip}, by solving the problem

$$\begin{cases} c^{n+1}\psi_e(\boldsymbol{u}^{n+1}_{tip}) = G\epsilon\Delta c^{n+1} + \dfrac{G}{\epsilon}(1-c^{n+1}) & \text{in } \Omega^n_{tip} \\ c^{n+1} = \dfrac{G}{G+2\epsilon\psi_e} & \text{on } \gamma^n_b \cup \gamma^n_d \; ; \\ \nabla c^{n+1}\cdot\boldsymbol{n} = 0 & \text{on } \gamma^n_a \cup \gamma^n_c \end{cases} \tag{14}$$

(e) Localize the new tip $\boldsymbol{x}^{n+1}_{tip}$ with (12) and update crack level set by adding the new crack segment that connects $\boldsymbol{x}^n_{tip}$ and $\boldsymbol{x}^{n+1}_{tip}$.

(f) Obtain Ω^{n+1}_{tip} by moving Ω^n_{tip} to maintain the tip domain centered at the crack tip.

5.2 Generalization to mixed-mode propagation

The implementation of the more general case of mixed mode propagation follows the same steps (a), (b), (c), (d), (e) and (f) described in Paragraph 5.1 and is summarized in Figure 9. However, specific attention should be payed in setting the boundary conditions in step (d), and in localizing the crack tip in step (e).

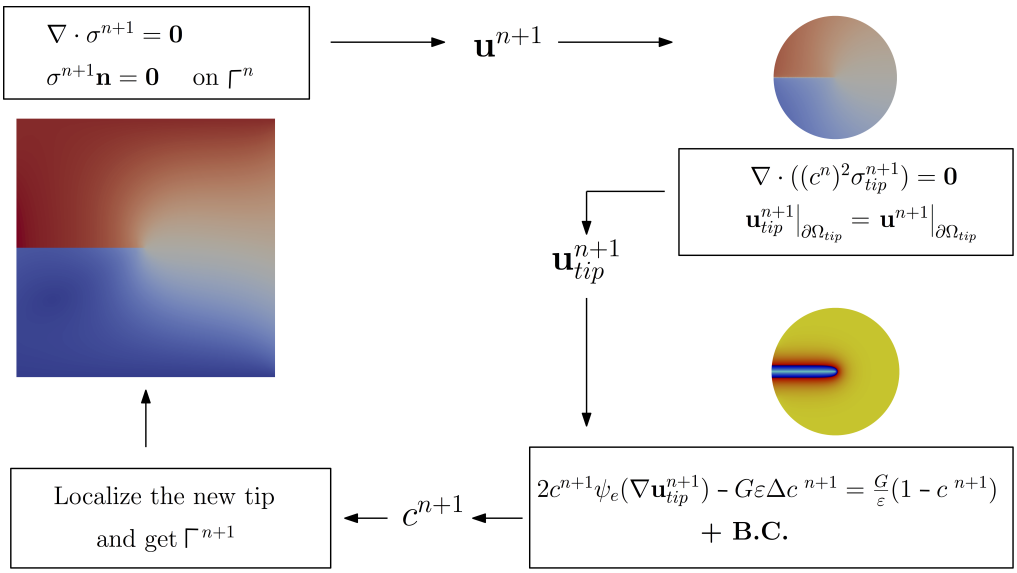

Figure 9: *A scheme of the Xfield method.*

As before, the crack is discretized as a set of segments, but these segments may now have different orientations from one to one another, and the propagation direction is not assumed to be known *a priori*. Since there is not a preferential propagation direction, for the sake of symmetry, we choose a circular tip domain instead of a square one.

As sketched in Figure 10, more than one crack segment is allowed to lie inside a single tip domain. As a consequence, see Figure 11, one cannot assume without lack

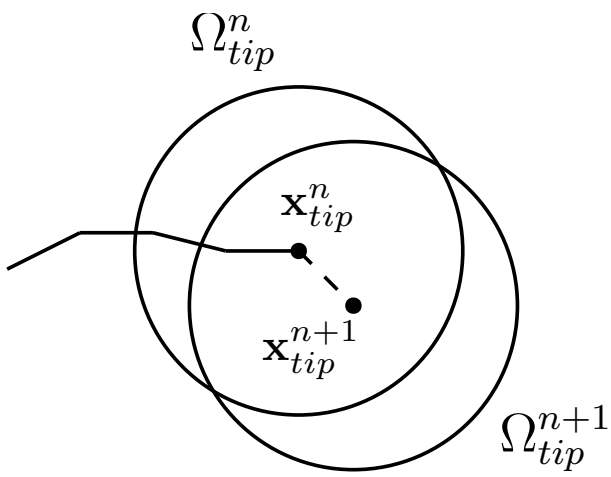

Figure 10: *The tip domain at two consecutive time iterations. The tip domain moves as the crack propagates, following the propagation of the crack.*

of generality that the crack segment that intersects the boundary of the tip domain is normal to the boundary itself, as it was done in the previous paragraph. Hence, it would not make sense to set on this portion of the boundary, namely γ_a in Figure 11, a homogeneous Neumann boundary condition for the phase field. A proper condition for the phase field on γ_a can be obtained assuming that the phase field behaves, in the direction orthogonal to the crack, as the analytic solution of the 1D differential equation

$$\begin{cases} -\epsilon\, c''(x) = \dfrac{1}{\epsilon}(1 - c(x)), \quad x \in (-\infty, \infty) \\ c(0) = 0 \\ \lim\limits_{x \to \pm\infty} c(x) = 1 \end{cases} .$$

Given a point $\boldsymbol{x}$ on γ_a, we compute its distance $d(\boldsymbol{x})$ from the crack segment that intersects the boundary of the tip mesh. The boundary condition on γ_a is then set as

$$c(\boldsymbol{x}) = 1 - \exp\left(-\frac{d(\boldsymbol{x})}{\epsilon}\right), \qquad \boldsymbol{x} \in \gamma_a.$$

The width of the boundary region γ_a can be chosen in such a way that the maximum distance between one point on the boundary and the crack segment intersected is 3ϵ, so that in the end points of γ_a one expects $c \approx 1$.

On the opposite part of the boundary with respect to the crack tip, that is γ_c, we set a homogeneous Neumann boundary condition, in order not to favor any direction of crack growth. The location of γ_c is chosen so that it is symmetric with respect to the point identified by the intersection of the extension of the last crack segment in Ω_{tip}, that is the segment ending at the corresponding tip. The length of the boundary region γ_c is here set to be one fourth of the length of the whole boundary.

Finally, on the remaining part of the boundary, that is $\gamma_b \cup \gamma_d$, we set the same Dirichlet condition of Paragraph 5.1, that is

$$c(\boldsymbol{x}) = \frac{G}{G + 2\epsilon\psi_e}, \qquad \boldsymbol{x} \in \gamma_b \cup \gamma_d.$$

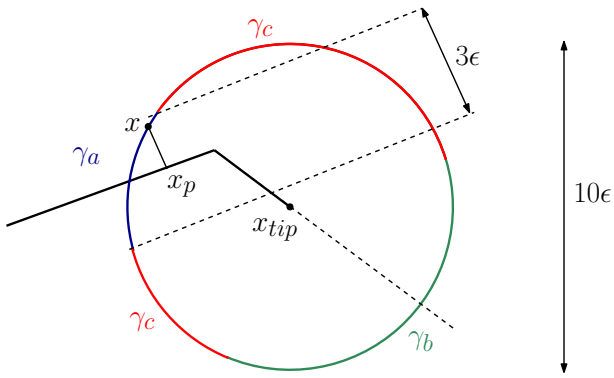

Figure 11: *The subdivision of the boundary of the circular tip mesh.*

Concerning step (e), the rigorous generalization of equation (12) for the crack tip localization from the phase field solution based on projections of ∇c along the tangent and normal direction of the crack will be subject of further work. We here mention that complications with this approach are due to the nonlinearity of the maximization problem

$$\boldsymbol{x}_{tip}^{n+1} = \arg \max_{\boldsymbol{x} \in \Omega_{tip}} \nabla c(\boldsymbol{x}) \cdot \boldsymbol{t}(\boldsymbol{x}), \tag{15}$$

being $\boldsymbol{t}(\boldsymbol{x})$ the tangent vector to the crack in point $\boldsymbol{x}$.

A more classical algorithm to identify a sharp crack path from a smeared description is, for example, the θ-simplified medial axis algorithm described in [35]. However, we have here implemented the mixed modes tip localization with a threshold criterion based on the value of c in the proximity of the previous crack tip.

6 Results

We have integrated the present method in a finite element code developed in *C++*, exploiting the open source library *GetFEM++* [36]. In all simulations, both the displacement field and the phase field are discretized with P1 elements. The direct solver *SuperLU* [37] is used for the solution of all the linear systems involved.

We apply the described procedure to the configuration represented in Figure 12. The tip domain used is circular and its diameter is 10ϵ long, as shown in Figure 11. A linearly increasing displacement load is applied to the top, as follows:

$$\tilde{\mathbf{u}} = \gamma t \begin{bmatrix} \cos\alpha \\ \sin\alpha \end{bmatrix}$$

where $\gamma = 10^{-5} m/s$ and $t \in (0, 3000s)$.

The loading condition of the crack is pure mode I if $\alpha = \pi/2$, pure mode II if $\alpha = 0$, and mixed modes if $\alpha \in (0, \pi/2) \cup (\pi/2, \pi)$.

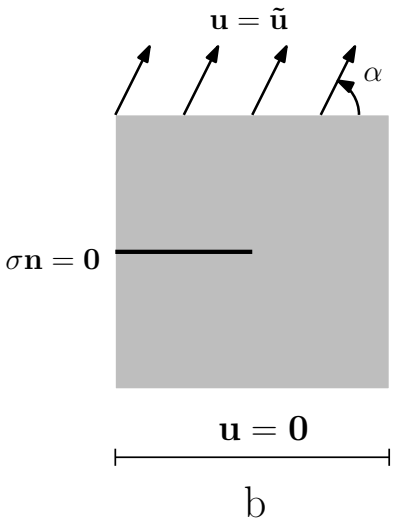

b	$1\ m$
λ	$120\ GPa$
μ	$80\ GPa$
G	$2700\ kN/m$
ϵ	$1.7\ 10^{-2}\ m$

Figure 12: The specimen is fixed at the bottom and subject at the top to an increasing displacement load. The parameters of the simulation are shown in the table.

We report in Figure 14 the displacement fields obtained with both the traditional phase field method with three different choices of ϵ on refined meshes accordingly, and the Xfield method, in the case $\alpha = \pi/2$, which corresponds to pure mode I.

The Xfield results show a delay of the onset of the propagation with respect to the phase field one and a slower propagation. However, the phase field propagation velocity decreases reducing the value of ϵ, consistently with the results in [34] and with the observation that the diffusion coefficient of the partial differential equation (10) is proportional to ϵ. Moreover, the propagation velocity does not seem to converge by reducing ϵ (reducing the mesh size h to maintain the same ratio ϵ/h). Hence it is not clear how to compare the propagation velocity of the Xfield with other results.

In Figure 13 the two meshes used for the solution of the far field displacement problem with the XFEM and for the coupled problem on the tip domain are shown. The former has a uniform element size of 30 mm, while the latter resolution is of 1 mm.

Figure 15 shows a mixed mode simulation for $\alpha = \pi/4$. On the left hand side the displacement field is reported, while on the right hand side the tip mesh in shown with the phase field solution. The crack in this case bends downwards and the tip mesh is always centered at tip and follows the propagation.

Figure 16 shows the phase field solutions on the tip mesh while the crack is bending, while Figure 17 shows the final configuration of the elstic material in the two numerical tests $\alpha = \pi/2$, on the left, and $\alpha = \pi/4$, on the right.

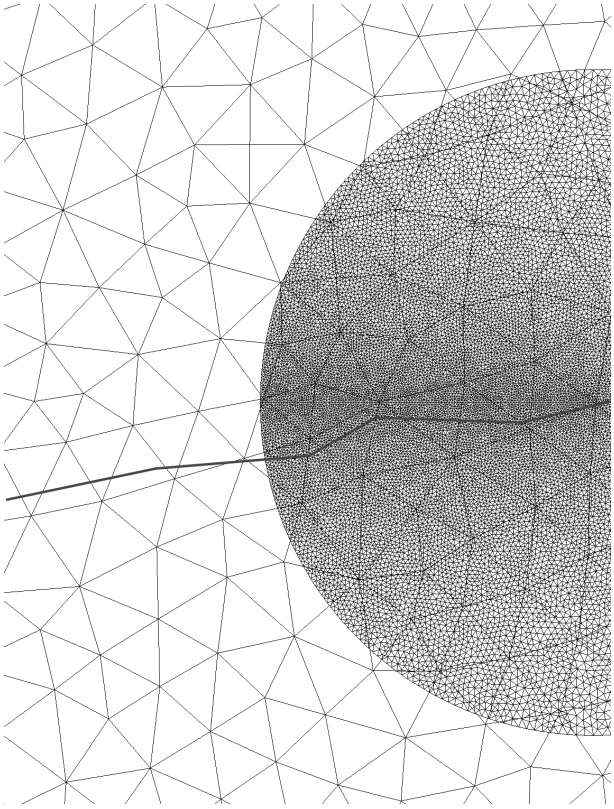

Figure 13: *The mesh for the tip domain is much finer than that used for the whole domain.*

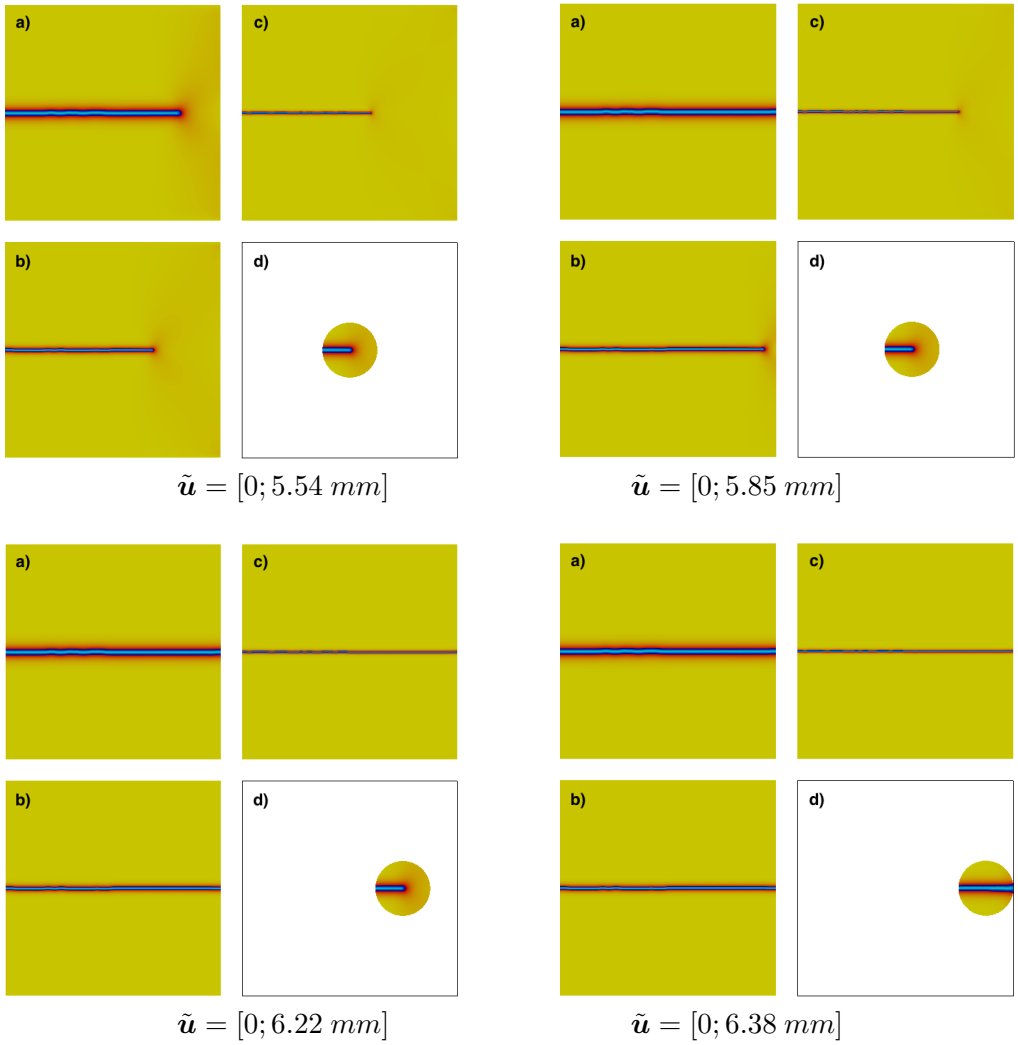

Figure 14: *The phase field variable c in mode I at four different load steps. Each subfigure contains a comparison of the traditional phase field solution obtained with three different ϵ, namely a) $\epsilon = 1.7\ 10^{-2}\ m$, b) $\epsilon = 0.85\ 10^{-2}\ m$, c) $\epsilon = 0.425\ 10^{-2}\ m$, and d) the Xfield with $\epsilon = 1.7\ 10^{-2}\ m$. The tip domain is shown at its correspondent position inside the domain. Notice the horizontal movement of the tip mesh, which follows the crack path.*

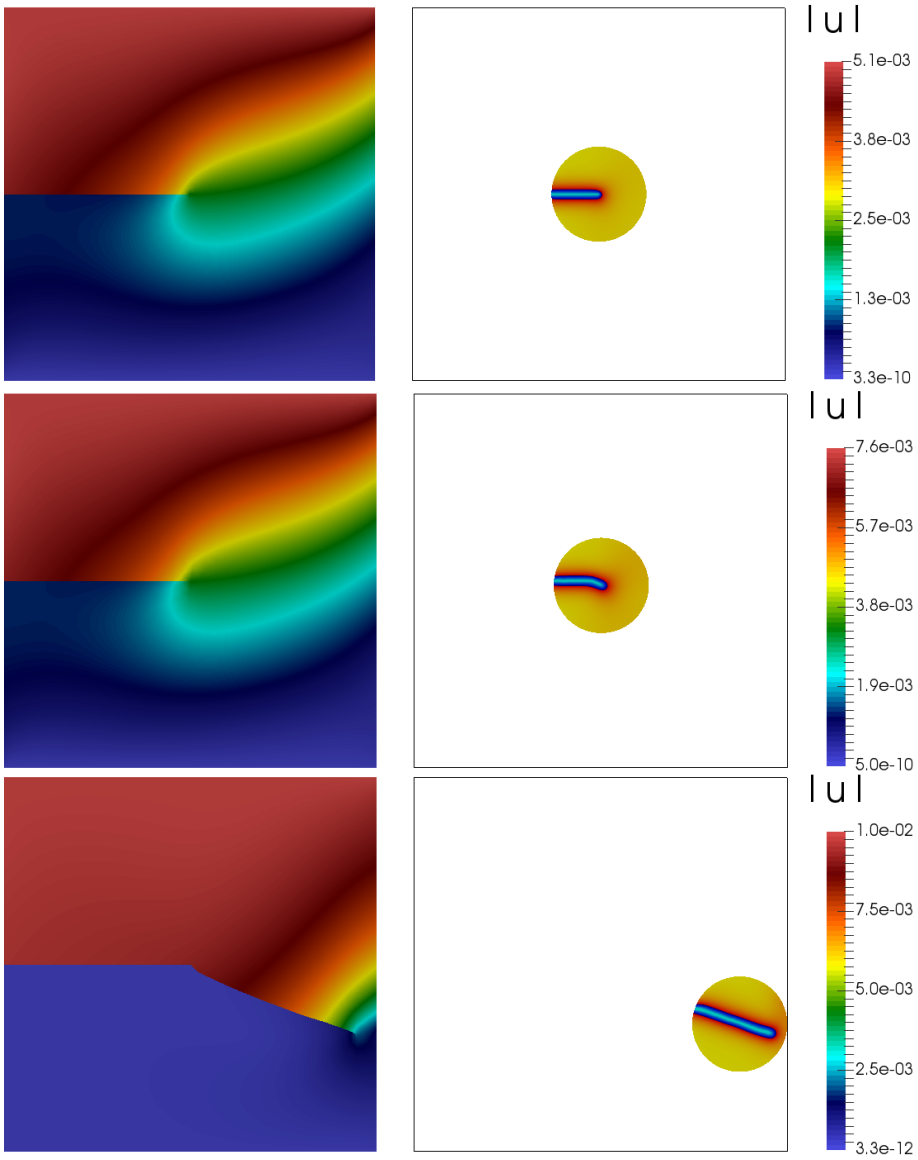

Figure 15: *The displacement and phase field obtained with the Xfield in mixed modes at different load steps. The tip mesh is shown on the right at its correspondent position inside the domain. Notice the movement of the tip mesh, which follows the crack path.*

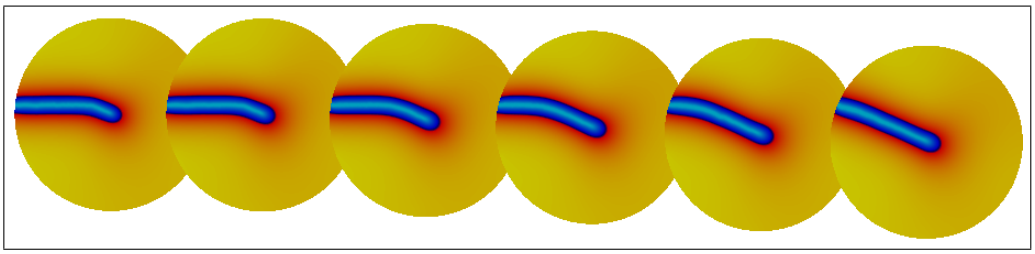

Figure 16: *The phase field solution on the tip mesh while the crack is bending. Note that the vertical displacement of the tip mesh is following the tip position, while the horizontal one is here enhanced for the sake of visualization.*

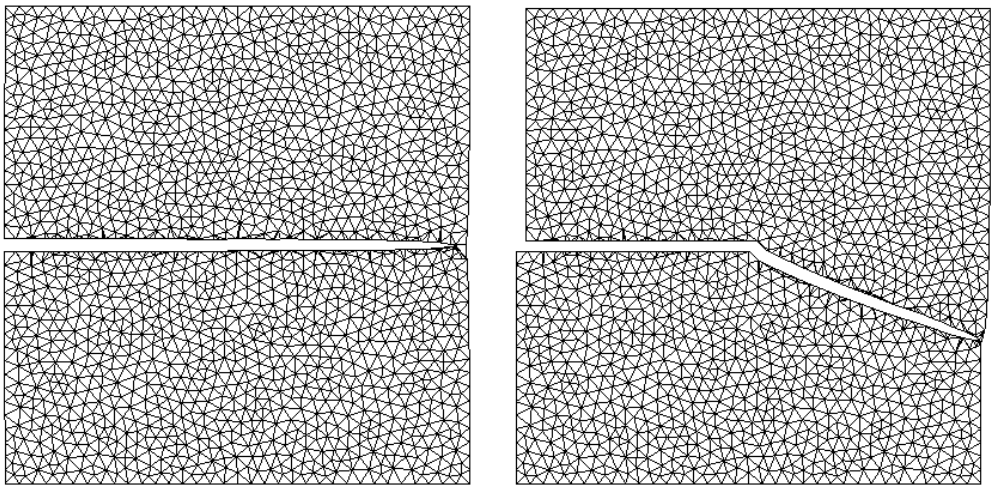

Figure 17: *The final configurations of the domain for* $\alpha = \pi/2$ *(left) and* $\alpha = \pi/4$ *(right).*

7 Conclusion

The aim of this work was to develop a novel method for the simulation of crack propagation with the following features:

- It is based on an energetic criterion;
- It does not require any mesh adaptation strategy, nor to know the crack path in advance to locally refine the mesh;
- It explicitly describes the crack opening;
- Its computational cost does not depend on the length scale ϵ introduced in phase field models.

A method compliant with these features was implemented and tested in simple mixed modes geometries. The developed method, called Xfield, well captures the direction of propagation. However it is not clear how to compare the propagation velocity with the results obtained with other traditional methods.

Further developments of this work include the extension of the method to more complex geometries and its improvement to account for crack initiation with a stress monitoring based criterion. Accounting for branching and merging cracks is possible but requires an extremely reliable algorithm for tip localization, which will be the subject of future work.

An interesting application to validate the Xfield in the future is the simulation of hydraulic fracture. Indeed, in this application a fluid is allowed to flow in the crack and an explicit and accurate description of the opening of the crack is crucial.

References

[1] T. Belytschko, T. Black, Elastic crack growth in finite element with minimal remeshing, International Journal for Numerical Methods in Engineering 45 (5) (1999) 601–620. doi:10.1002/(SICI)1097-0207(19990620)45:5<601::AID-NME598>3.0.CO;2-S.

[2] N. Moës, J. Dolbow, T. Belytschko, A finite element method for crack growth without remeshing, International Journal for Numerical Methods in Engineering 46 (1) (1999) 131–150. doi:10.1002/(SICI)1097-0207(19990910)46:1<131::AID-NME726>3.0.CO;2-J.

[3] J. Chessa, T. Belytschko, An enriched finite element method and level sets for axisymmetric two-phase with surface tension, International Journal for Numerical Methods in Engineering 58 (13) (2003) 2041–2064. doi:10.1002/nme.946.

[4] J. Chessa, T. Belytschko, An Extended Finite Element Method for Two-Phase Fluids, Journal of Applied Mechanics 70 (1) (2003) 10. doi:10.1115/1.1526599.

[5] A. Zilian, A. Legay, The enriched space–time finite element method (EST) for simultaneous solution of fluid–structure interaction, International Journal for Numerical Methods in Engineering 75 (3) (2008) 305–334. doi:10.1002/nme.2258.

[6] P. Gupta, C. A. Duarte, Simulation of non-planar three-dimensional hydraulic fracture propagation, International Journal for Numerical and Analytical Methods in Geomechanics 38 (13) (2014) 1397–1430. doi:10.1002/nag.

[7] G. A. Francfort, J.-J. Marigo, Revisiting brittle fracture as an energy minimization problem, Journal of the Mechanics and Physics of Solids 46 (8) (1998) 1319–1342. doi:10.1016/S0022-5096(98)00034-9.

[8] B. Bourdin, G. A. Francfort, J.-J. Marigo, The Variational Approach to Fracture, Journal of Elasticity 91 (1-3) (2008) 5–148. doi:10.1007/s10659-007-9107-3.

[9] B. Bourdin, G. A. Francfort, J.-J. Marigo, Numerical experiments in revisited brittle fracture, Journal of the Mechanics and Physics of Solids 48 (4) (2000) 797–826. doi:10.1016/S0022-5096(99)00028-9.

[10] B. Bourdin, Numerical implementation of the variational formulation for quasi-static brittle fracture, Interfaces and Free Boundaries 9 (3) (2007) 411–430. doi:10.4171/IFB/171.

[11] V. Ziaei-Rad, Y. Shen, Massive parallelization of the phase field formulation for crack propagation with time adaptivity, Computer Methods in Applied Mechanics and Engineering. (2016) doi:10.1016/j.cma.2016.04.013.

[12] M. F. Wheeler, T. Wick, W. Wollner, An augmented-Lagrangian method for the phase-field approach for pressurized fractures, Computer Methods in Applied Mechanics and Engineering 271 (2014) 69–85. doi:10.1016/j.cma.2013.12.005.

[13] E. Gordeliy, A. Peirce, Enrichment strategies and convergence properties of the XFEM for hydraulic fracture problems, Computer Methods in Applied Mechanics and Engineering 283 (2015) 474–502. doi:10.1016/j.cma.2014.09.004.

[14] S. N. Roth, P. Léger, A. Soulaïmani, A combined XFEM-damage mechanics approach for concrete crack propagation, Computer Methods in Applied Mechanics and Engineering 283 (2015) 923–955. doi:10.1016/j.cma.2014.10.043.

[15] G. Zi, J. Song, E. Budyn, S. Lee, T. Belytschko, A method for growing multiple cracks without remeshing and its application to fatigue crack growth, Modelling and Simulation in Materials Science and Engineering 12 (5) (2004) 901–915. doi:10.1088/0965-0393/12/5/009.

[16] É. Budyn, G. Zi, N. Moes, T. Belytschko, A method for multiple crack growth in brittle materials without remeshing, International Journal for Numerical Methods in Engineering 61 (10) (2004) 1741–1770. doi:10.1002/nme.1130.

[17] C. Daux, N. Moes, J. Dolbow, Arbitrary branched and intersecting cracks with the extended finite element method, International Journal for Numerical Methods in Engineering 48 (12) (2000) 1741–1760. doi:10.1002/1097-0207(20000830)48:12<1741::AID-NME956>3.0.CO;2-L.

[18] T. Belytschko, N. Moes, S. Usui, C. Parimi, Arbitrary discontinuities in finite elements, International Journal for Numerical Methods in Engineering 50 (4) (2001) 993–1013. doi:10.1002/1097-0207(20010210)50:4<993::AID-NME164>3.0.CO;2-M.

[19] P. M. A. Areias, T. Belytschko, Analysis of three-dimensional crack initiation and propagation using the extended finite element method, International Journal for Numerical Methods in Engineering 63 (5) (2005) 760–788. doi:10.1002/nme.1305.

[20] D. Colombo,An implicit geometrical approach to level sets update for 3D non planar X-FEM crack propagation, Computer Methods in Applied Mechanics and Engineering 237-240 (2012) 39–50. doi:10.1016/j.cma.2012.04.020.

[21] E. Chahine, P. Laborde, Y. Renard, Crack tip enrichment in the XFEM using a cut-off function, International Journal for Numerical Methods in Engineering 75 (6) (2008) 629–646. doi:10.1002/nme.2265.

[22] G. R. Irwin, Analysis of stresses and strains near the end of a crack traversing a plate, Journal of applied mechanics 24 (1957) 361–264.

[23] F. Erdogan, G. C. Sih, On the Crack Extension in Plates Under Plane Loading and Transverse Shear (1963). doi:10.1115/1.3656897.

[24] G. C. Sih, Strain-energy-density factor applied to mixed mode crack problems, International Journal of Fracture 10 (3) (1974) 305–321. doi:10.1007/BF00035493.

[25] M. Hussain, S. Pu, J. Underwood, Strain energy release rate for a crack under combined Mode I and Mode II, in: Proceedings of the 1973 National Symposium on Fracture Mechanics, 1973. doi:10.1520/STP33130S.

[26] J. R. Rice, Mathematical analysis in the mechanics of fracture, Fracture: an advanced treatise 2 (1968) 191–311.

[27] J. R. Rice, A Path Independent Integral and the Approximate Analysis of Strain Concentration by Notches and Cracks, Journal of applied mechanics 35 (1968) 379–386.

[28] A. Griffith, The phenomena of rupture and flow in solids, Philosophical Transactions of the Royal Society of London.

[29] G. A. Francfort, C. Larsen, Existence and convergence for quasi-static brittle evolution in brittle fracture, Communications on Pure and Applied Mathematics 56 (10) (2003) 1465–1500. doi:10.1002/cpa.3039.

[30] L. Ambrosio, V. M. Tortorelli, Approximation of Functionals Depending on Jumps by Elliptic Functionals via Gamma-Convergence, Communications on Pure and Applied Mathematics 43 (1991) 999–1036.

[31] A. Giacomini, Ambrosio-Tortorelli approximation of quasi-static evolution of brittle fractures, Calculus of Variations and Partial Differential Equations 22 (2) (2005) 129–172. doi:10.1007/s00526-004-0269-6.

[32] S. Burke, C. Ortner, E. S. Uli, An Adaptive Finite Element Approximation of a Variational Model of Brittle Fracture, SIAM Journal on Numerical Analysis. 48 (3) (2010) 980–1012. doi:10.1142/S021820251350019X.

[33] M. Artina, M. Fornasier, S. Micheletti, S. Perotto, Anisotropic mesh adaptation for crack detection in brittle materials, SIAM Journal on Scientific Computing 37 (4) (2015) B633–B659. doi:10.1137/140970495.

[34] C. Miehe, M. Hofacker, F. Welschinger, A phase field model for rate-independent crack propagation: Robust algorithmic implementation based on operator splits, Computer Methods in Applied Mechanics and Engineering 199 (45-48) (2010) 2765–2778. doi:10.1016/j.cma.2010.04.011.

[35] E. Tamayo-Mas, A. Rodríguez-Ferran, A medial-axis-based model for propagating cracks in a regularised bulk, International Journal for Numerical Methods in Engineering 101 (7) (2015) 489–520. doi:10.1002/nme.

[36] Y. Renard, J. Pommier. GetFem++5.1 (2016).

[37] J. W. Demmel, S. C. Eisenstat, J. R. Gilbert, X. S. Li, J. W. H. Liu, A supernodal approach to sparse partial pivoting, SIAM Journal on Matrix Analysis and Applications 20 (3) (1999) 720-755.